Energy Bands in Ferromagnetic Nickel†

Julius Langlinais and Joseph Callaway
Department of Physics, Louisiana State University, Baton Rouge, Louisiana 70803
(Received 17 June 1971)

The tight-binding method has been employed to calculate energy bands in ferromagnetic nickel. The basis set consisted of atomic wave functions for the $1s$, $2s$, $3s$, $4s$, $2p$, $3p$, and $4p$ states, expressed as linear combinations of Gaussian orbitals, and five individual Gaussian orbitals for each $3d$ state. The Coulomb part of the crystal potential was constructed from a superposition of overlapping neutral-atom charge densities, the atoms being in the d^9s^1 configuration. The $X\alpha$ method of Slater *et al.* was used to construct an exchange potential. Energy levels were calculated at 1505 points in $\frac{1}{48}$th of the Brillouin zone. The results are generally in good agreement with those obtained from other first-principles calculations. The properties for several positions on the Fermi surface are determined and compared with experiment. The spin splitting of the d bands is calculated to be about 0.8 eV. A spin-wave reciprocal effective mass of 0.165 (in atomic units) is obtained.

I. INTRODUCTION

The relation between band structure and ferromagnetism has long presented a challenge to the theory of solids. The study of the properties of nickel has been of considerable importance for the theory of ferromagnetism, since it appears to be the simplest of the $3d$ elemental ferromagnets. Substantial information is available concerning the Fermi surface of nickel as well as its magnetic properties.

There have been many calculations of energy bands in nickel.[1-16] With the exception of some preliminary work using the tight-binding[1,2,4,16] method, and one $\vec{k}\cdot\vec{p}$ study,[12] these calculatations have used the augmented-plane-wave (APW) method,[3,6,8,11,14] the Green's-function method,[4,5,7] or the combined interpolation scheme.[9,10,13-15] Thus the majority of these calculations have either been semiempirical in nature, or have used a "muffin-tin" form of crystal potential. There are, however, reasons to question the adequacy of approaches based on approximations in which the crystal potential at each atomic site is spherically symmetric in application to d bands. Crystal-field effects are neglected. While probably small, they may not be entirely negligible.[17] Specifically, predictions of the Fermi surface in nickel depend sensitively on the position of the levels X_5 and X_2 at the center of a square face of the Brillouin zone. The separation of these levels will be influenced by the presence of a term in the crystal potential around each atom having cubic, rather than spherical, symmetry.

We have decided to apply the tight-binding method, as improved by Lafon and Lin,[18] to the band structure of nickel. In its present form, the method seems to be as accurate as other methods, and in addition does not necessarily incorporate restrictive assumptions about the symmetry of the crystal potential. The elements of the Hamiltonian and overlap matrices are independent of energy so that all the energy values can be found by a standard diagonalization procedure. The size of the matrices which must be considered is small enough (here 38×38) so that energies can be obtained at a moderate number of general points in the Brillouin zone without an unduly large expenditure of computer time.

The present calculation determined energy levels at 1505 points in $\frac{1}{48}$th of the Brillouin zone. The investigation was based on an assumed crystal potential constructed from a superposition of overlapping neutral-atom charge densities, the atoms being in the d^9s^1 configuration. This potential is not of the muffin-tin form, and it is not spherically symmetric in an atomic cell. Exchange was included according to the "$X\alpha$" method of Slater, Wilson, and Wood.[19] This prescription was also used to consider the exchange splitting of the energy bands in the ferromagnetic state. Spin-orbit coupling was neglected here, but will be considered in further work.

The results are compared with those obtained by other methods, and with experiment. Areas are presented for significant cross sections of the Fermi surface. The spin-wave reciprocal effective mass is computed in a simple approximation. In general, the results demonstrate that the tight-binding method can yield a band structure for a transition metal at least comparable in accuracy to those obtained by other methods of band-structure calculations. The agreement with experiment is satisfactory, although not as good as can be obtained by semiempirical interpolation schemes which have been designed to enable an accurate fit to experimental data. The characteristics of the present form of the tight-binding method are clarified by this investigation and the requirements for

successful application become apparent. We believe that tight-binding calculations can be made self-consistent.[20] An attempt is in progress to achieve self-consistency for nickel.

II. TIGHT-BINDING METHOD

In this section, we review the essential features of the tight-binding method as reformulated by Lafon and Lin.[18]

We begin with a set of localized basis functions $u_j(\vec{r})$. For convenience, these functions will be assumed to be normalized, but need not be orthogonal. In conventional descriptions of the tight-binding method, the u_j's are chosen to be wave functions for states of the free atoms of which the crystal is composed. This procedure is not necessary and may be too restrictive. In this work, some of the u_j will be atomic functions, others will be individual localized (Gaussian-type) orbitals.

In the first step, linear combinations of the $u_j(\vec{r})$ are constructed which satisfy Bloch's theorem for wave vector $\vec{k}$. Let these be denoted $\phi_j(\vec{k}, \vec{r})$:

$$\phi_j(\vec{k}, \vec{r}) = (1/N^{1/2}) \sum_\mu e^{i\vec{k}\cdot\vec{R}_\mu} u_j(\vec{r} - \vec{R}_\mu) . \quad (2.1)$$

For convenience, we restrict our attention to a crystal with one atom per unit cell, the direct-lattice vectors being denoted by $\vec{R}_\mu$. We require the Hamiltonian and overlap matrices on the basis of the $\phi_j(\vec{k}, \vec{r})$.

The present approach differs from more conventional applications of the tight-binding method in the treatment of the Hamiltonian. If the crystal potential $V_c(\vec{r})$ is expressed as the sum of individual atomic potentials $V_A(\vec{r} - \vec{R}_\mu)$, one finds it necessary to compute three-center integrals of the form

$$\int u_j(\vec{r}) V_A(\vec{r} - \vec{R}_\mu) u_n(\vec{r} - \vec{R}_\nu)\, d^3r . \quad (2.2)$$

The computation of integrals of this type has been a major obstacle to quantitative development of the tight-binding method.

Instead of expressing the crystal potential as a sum of atomic potentials, we will use a Fourier representation

$$V_c(\vec{r}) = \sum_s V(\vec{K}_s) e^{i\vec{K}_s\cdot\vec{r}} \quad (2.3)$$

in which the $\vec{K}_s$ are reciprocal-lattice vectors. We note that each term in the sum, as well as the complete potential, is unchanged by displacement through a direct-lattice vector. For this reason, three-center integrals do not appear.

Let T denote the kinetic-energy term in the Hamiltonian. The matrix elements of the Hamiltonian are

$$H_{jn}(\vec{k}) = \int \phi_j(\vec{k}, \vec{r}) [T + V_c(\vec{r})] \phi_n(\vec{k}, \vec{r})\, d^3r$$
$$= \sum_\mu e^{i\vec{k}\cdot\vec{R}_\mu} [T_{jn}(\vec{R}_\mu) + \sum_s V(\vec{K}_s) s_{jn}(\vec{k}, \vec{K}_s)] . \quad (2.4)$$

The $s_{jn}(\vec{k}, \vec{K}_s)$ can be expressed as

$$s_{jn}(\vec{k}, \vec{K}_s) = \sum_\mu e^{i\vec{k}\cdot\vec{R}_\mu} S_{jn}(\vec{K}, \vec{R}_\mu) , \quad (2.5)$$

in which

$$S_{jn}(\vec{K}, \vec{R}_\mu) = \int u_j(\vec{r}) e^{i\vec{K}\cdot\vec{r}}\, u_n(\vec{r} - \vec{R}_\mu)\, d^3r . \quad (2.6)$$

The elements of the overlap matrix can be determined from (2.5) simply by setting $K = 0$. The quantity $T_{jn}(\vec{R}_\mu)$ is a matrix element of the kinetic-energy operator. In a crystal with a center of inversion, it is sufficient to consider integrals similar to (2.6) with $\cos(\vec{K}\cdot\vec{r})$ replacing $e^{i\vec{K}\cdot\vec{r}}$.

Equation (2.4) may be written in an alternative manner,

$$H_{jn}(\vec{k}) = \sum_\mu e^{i\vec{k}\cdot\vec{R}_\mu} E_{jn}(\vec{R}_\mu) , \quad (2.7)$$

in which

$$E_{jn}(\vec{R}_\mu) = T_{jn}(\vec{R}_\mu) + V_{jn}(\vec{R}_\mu) \quad (2.8)$$

and $V_{jn}(\vec{R}_\mu)$ is given by

$$V_{jn}(\vec{R}_\mu) = \sum_s V(\vec{K}_s) S_{jn}(\vec{K}_s, \vec{R}_\mu) . \quad (2.9)$$

The fundamental computational problem in the present approach to the tight-binding method is the calculation of integrals of the type $S_{jn}(\vec{K}, \vec{R})$ appearing in (2.5). A very large number of such integrals are required (of the order of 10^7). For this reason, it is essential to simplify the determination of these quantities as much as possible. To this end, we have decided to work with Gaussian-type orbitals (GTO) as suggested by Chaney, Tung, Lin, and Lafon.[21] The advantage of such orbitals is that analytic expressions can be obtained for all of the $S_{jn}(\vec{K}, \vec{R})$. The specific expressions used are given in Appendix A.

The use of GTO's is open to the criticism that the representation of an atomic wave function in terms of such orbitals is more cumbersome than with Slater-type orbitals (STO). More GTO's than STO's must be included to obtain a similar degree of accuracy. This criticism is justified, but we believe that it is outweighed by the superior ease of calculation with GTO's. Analytic expressions for the S_{jn} are not known on an STO basis; instead a rather intricate numerical integration must be performed. We do not believe that an accurate tight-binding calculation for a crystal composed of atoms with as many electrons as nickel is practical with a basis set of STO's.

We used the following specific set of basis functions in this calculation. Wave functions for all atomic states except $3d$ (e.g., $1s$, $2s$, $3s$, $4s$, $2p$, $3p$, and $4p$) were represented by the linear combinations of Gaussian orbitals determined from a free-atom self-consistent-field calculation by Wachters.[22] Inclusion of core wave functions is necessary (just as in the orthogonalized-plane-wave method) in order to avoid convergence difficulties

associated with the lack of orthogonality of wave function on different atom. The accuracy of the representation of the 4s and 4p states in terms of atomic functions is perhaps questionable; however, previous experience with the tight-binding method[18,21] shows that excellent results can be obtained for s and p bands in alkali metals by this procedure.

On the other hand, we have seen some evidence in a preliminary calculation[16] that the d-electron wave functions in the solid may be appreciably different from those existing in the free atom. In order to allow for this possibility we used a set of five separate radial GTO (for each type of angular dependence) in the construction of the $\phi_j(\vec{k}, \vec{r})$. The orbital exponents used in defining these functions were the same as used by Wachters.[22]

With this choice of basis functions, we obtain a 38×38 matrix problem at a general point of the Brillouin zone. The d–d portion is 25×25, the p–p portion 9×9, and the s–s portion 4×4. With matrices of this size, it is possible to obtain energy levels at a reasonably large number of general points in the Brillouin zone.

The computation of the matrix elements H_{jn} involves a double summation, and convergence must be achieved in both. The degree of difficulty depends on the orbitals involved. Terms of s–s and s–p types present the greatest problem. Near a nucleus, s-like wave functions are sharply peaked and p-like functions have a large gradient. As a result, the summation over reciprocal-lattice vectors requires many terms. For example, approximately 8100 rotationally independent reciprocal-lattice vectors were included in sums for the s–s elements for the first five neighbors. As the results were still not entirely converged, the remainder of the sum was replaced by an integral, which was evaluated using Filon's rule. An example of the convergence of such a summation is shown in Fig. 1. Much more rapid convergence was obtained for elements involving d functions.

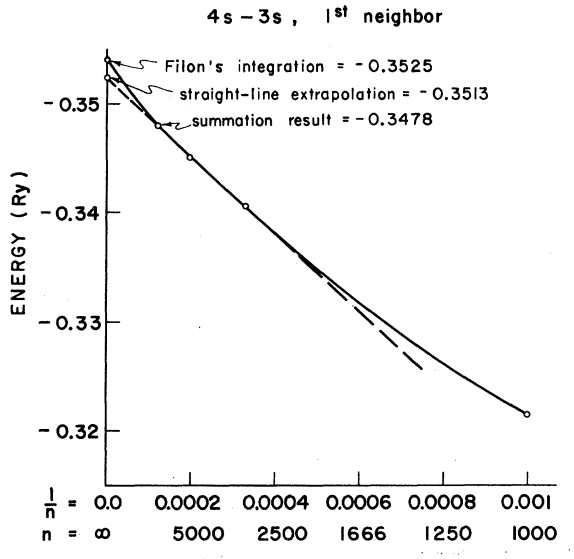

FIG. 1. Convergence of the nearest-neighbor 3s–4s element $V_{3s,4s}$ $[\frac{1}{2}a(1, 1, 0)]$ (in which V represents the ordinary Coulomb potential) is shown as a function of $1/N$, where N is the number of independent reciprocal-lattice vectors included in the sum (2.8). The sum was carried to approximately $N=8100$; the remainder was estimated both graphically, and by integrating the Fourier series.

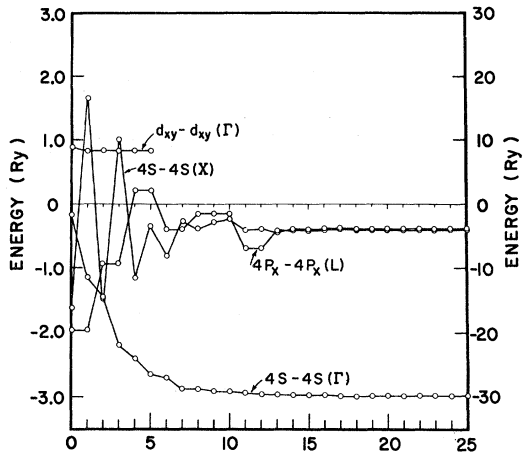

FIG. 2. Convergence of the sum (2.7) is shown for certain matrix elements as a function of the number of shells of direct-lattice vectors included. Four matrix elements 4s–4s [(Γ) and (X)], $4p_x-4p_x(L)$, and $d_{xy}-d_{xy}(\Gamma)$ are studied. The last case involves the most extended d orbital.

The 4s and 4p wave functions are highly extended in space. It was necessary to include 40 shells of neighbors (rotationally independent vectors $\vec{R}_\mu$) in order to obtain convergence. There is, unfortunately, substantial cancellation in the computation of certain matrix elements. The d–d matrix elements converged much more rapidly. Only five shells of neighbors were required in this case. The $\vec{R}$ convergence of certain matrix elements is shown in Fig. 2.

III. CRYSTAL POTENTIAL

The crystal potential was constructed as follows: It was assumed that the charge density of electrons in the crystal could be replaced as a superposition of partially overlapping charge densities for individual nickel atoms in a $3d^9 4s^1$ configuration. The individual atomic charge densities were chosen to be spherically symmetric; however, the superposed density has only cubic symmetry about any lattice site. The wave functions used in forming the charge density were taken from the Hartree-Fock

self-consistent field calculation of Clementi[23] for the free nickel atom in the $3d^8 4s^2(^3F)$ configuration.

The Fourier coefficients of the Coulomb potential for this model are given by the expression below (atomic units with energies in rydbergs are used throughout this paper):

$$V(K) = \frac{-8\pi}{\Omega K^2}\left(Z - K^{-1}\sum_{nl} a_{nl}\int_0^\infty r R_{nl}^2(r)\sin Kr\, dr\right) \tag{3.1}$$

in which Z is the atomic number, Ω is the volume of the unit cell, a_{nl} specifies the occupancy of the shell nl, and R_{nl} is the radial part of the wave function for this shell. These integrals may be readily evaluated analytically.

A local exchange potential was constructed using the $X\alpha$ method of Slater, Wilson, and Woods,[19]

$$V_{ex,\sigma}(\vec{r}) = -6\alpha[(3/4\pi)\rho_\sigma(\vec{r})]^{1/3}. \tag{3.2}$$

In this expression ρ_σ is the total charge density of electrons of spin σ. The charge density above was constructed by adding the overlapping distributions produced by neutral atoms in the configuration mentioned above placed on the appropriate lattice sites. The original Slater exchange potential[24] has $\alpha = 1$; the Kohn-Sham-Gaspar[25] potential has $\alpha = \frac{2}{3}$. In the present calculation, we investigated the effects of the variation of α between these limits. The results appeared to be more satisfactory when α was close to unity. The determination of the actual value used is described subsequently.

The Slater approximation for an effective exchange potential can be used to investigate the band structure of a ferromagnetic metal. The exchange potential for an electron of given spin is determined by the electron distribution for that spin. When the number of electrons in states of ↑ and ↓ spin are

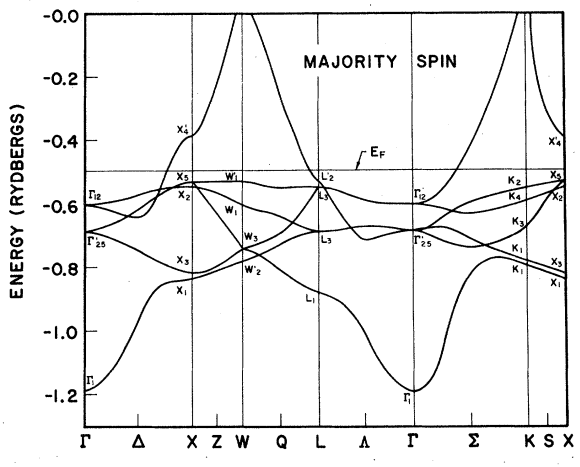

FIG. 3. Band structure for majority-spin states along certain symmetry directions. The horizontal line at −0.492 Ry indicates the position of the Fermi energy.

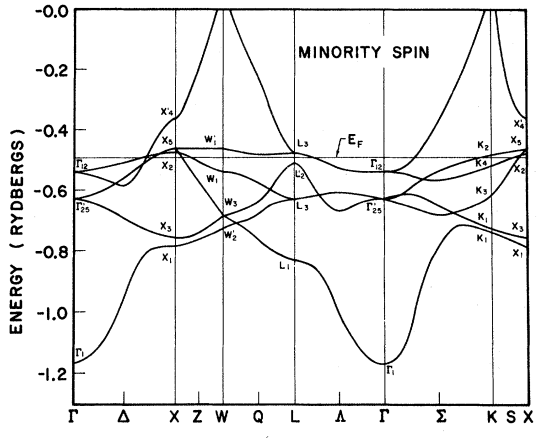

FIG. 4. Band structure for minority-spin states along certain symmetry directions. The horizontal line at −0.492 Ry indicates the position of the Fermi energy.

different, the exchange potential will tend to cause a splitting of the band structure. This approach was first applied in a study of energy bands in ferromagnetic iron by one of us,[26] and has subsequently been employed by Wakoh[7] and Connolly[11] in studies of nickel. We assumed here that the magneton number was 0.56, and that this was entirely produced by the d electrons. For the assumed d^9s^1 configuration, this implies that we should have 4.78 d electrons of majority (↑) spin, and 4.22 d electrons of minority (↓) spin. This assumption was used to construct the exchange potentials.

This procedure has been criticized by Herring[27] and others who argue that an electron in a ferromagnetic metal cannot be regarded as experiencing an average exchange potential originating from atoms, all of which are in the same average configuration. Alternate procedures based on an approximate treatment of electron correlation in narrow bands have been employed.[9,15]

In view of the criticisms of Slater's procedure, it may be surprising that the results, at least in the case of nickel, are in fair agreement with other approaches[9,15] and with experiment. For example, Connolly[11] obtains a magneton number of 0.62 (in comparison with the experimental value of 0.56). Our result is not greatly different.

The parameter α was chosen in the following way: It was observed that the relative position of the p- and d-like levels at the Brillouin-zone point L was quite sensitive to the value of α. This occurs because the d-band level L_3 varies considerably more rapidly with α than the p-like state L_2'. There is experimental evidence indicating that $L_2'(\uparrow)$ should be about 0.4 eV below the Fermi energy. This is achieved for $\alpha \simeq 0.972$, which was the value adopted.

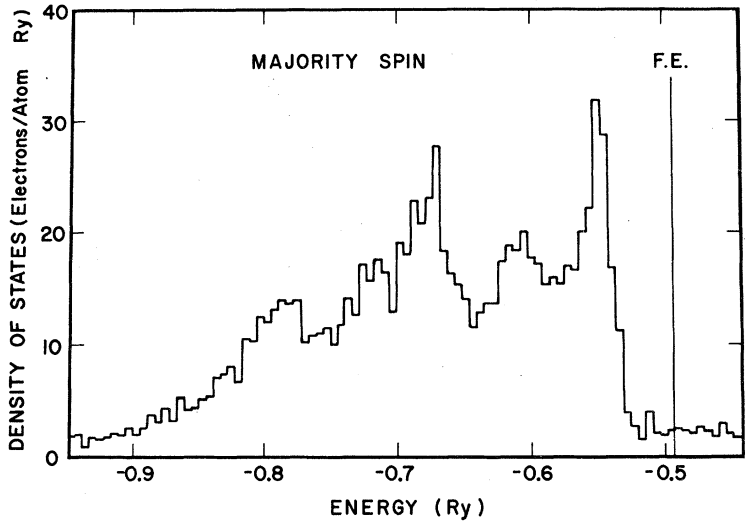

FIG. 5. Density of states for majority spin.

IV. RESULTS

Energy levels for both ↑ and ↓ spins were obtained at 1505 independent points in $\frac{1}{48}$th of the Brillouin zone. Portions of the band structures for majority (↑) and minority (↓) spins are shown in Figs. 3 and 4, respectively. The results are qualitatively similar to those obtained by Connolly[11] and others. The band structure shows the characteristic interlacing d bands, partially hybridized with an overlapping broad s–p band. A p state L_2' enters the d-band region at the center of a hexagonal zone face.

Certain characteristic energy differences between states are listed in Table I. The separation X_5–X_1 is a rough measure of the d bandwidth, while the Γ_1–X_4' separation gives the width of the overlapping s–p band. A significant feature of the band structure of nickel is the very flat highest d band, connecting the states X_5 and W_1'. If only nearest-neighbor interactions were considered, this band would be absolutely flat. Second-neighbor and higher-order interactions produce a slight deviation of $\epsilon(\vec{k})$ from constancy, but this is quite small: The energy variation between these states is only 4×10^{-5} Ry.

Some values for the energy differences between states of ↑ and ↓ spin are specified in Table II. It will be seen that, while the splitting of d-like states is not constant, it does not appear to vary very much, remaining in the neighborhood of 0.06 Ry or 0.8 eV. On the other hand, the splitting of predominantely s- and p-like states tends to be smaller by a factor of approximately 3. The present results for the spin splitting of d-like states are in reasonable agreement with those obtained in a previous calculation using t-matrix techniques[15] and also with those obtained by other authors using the Slater procedure.[7,11] Our result is, however, larger (by a factor of approximately 2) than values considered by Zornberg[14] as giving reasonable agreement with optical measurements.

A rough density of states was obtained by simple state counting techniques. Results for majority, minority, and total densities are presented in Figs. 5–7. The structure in the ↑ and ↓ d band densities are nearly the same except for a shift in energy corresponding to the spin splitting.

The Fermi energy was determined from the density of states. The magneton number, which is

TABLE I. Some characteristic energy differences (Ry).

	Majority spin	Minority spin
$\Gamma_{25'}-\Gamma_1$	0.506	0.544
$\Gamma_{12}-\Gamma_{25'}$	0.084	0.087
X_5-X_1	0.324	0.324
X_5-X_2	0.016	0.017
$X_{4'}-X_5$	0.144	0.101
$L_{2'}-L_{32}$	0.016	−0.029
$X_{4'}-\Gamma_1$	0.807	0.808
$W_{1'}-W_1$	0.074	0.078
$W_{1'}-X_5$	$\sim4\times10^{-5}$	$\sim4\times10^{-5}$

TABLE II. Some characteristic spin splittings (Ry).

$\Gamma_1(\downarrow)-\Gamma_1(\uparrow)$	0.022
$\Gamma_{25'}(\downarrow)-\Gamma_{25'}(\uparrow)$	0.060
$\Gamma_{12}(\downarrow)-\Gamma_{12}(\uparrow)$	0.063
$X_1(\downarrow)-X_1(\uparrow)$	0.054
$X_5(\downarrow)-X_5(\uparrow)$	0.066
$L_{32}(\downarrow)-L_{32}(\uparrow)$	0.065
$L_{2'}(\downarrow)-L_{2'}(\uparrow)$	0.020
$X_{4'}(\downarrow)-X_{4'}(\uparrow)$	0.023

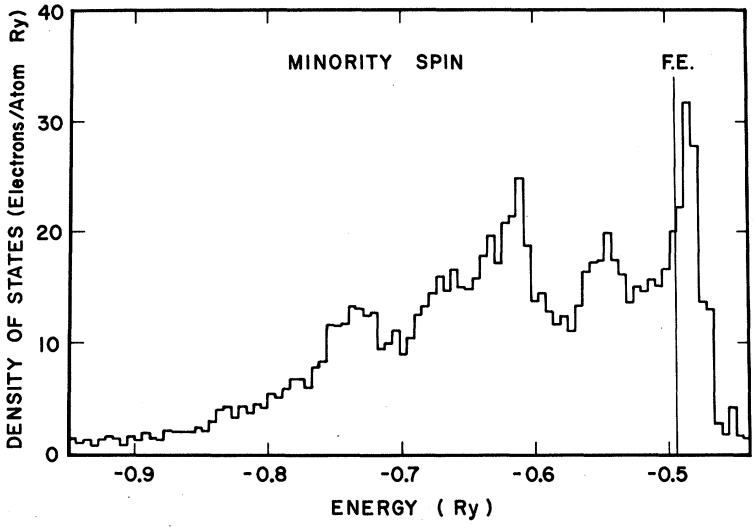

FIG. 6. Density of states of minority spin.

the difference between the number of occupied states of majority spin and the number of occupied minority spin states, was found to be 0.69. This is somewhat larger than the experimental value of 0.56.[28] The total density of states at the Fermi energy is 24 electrons/atom Ry.

Determination of the Fermi energy makes possible investigation of the Fermi surface. Certain cross sections of the predicted Fermi surface are shown in Figs. 8 and 9 which refer to majority and minority spins, respectively. Some properties of the Fermi surface are listed in Table III.

The majority-spin portion of the Fermi surface lies entirely in the upper (s–p) band 6. Qualitatively, it is similar to the Fermi surface of copper: a distorted sphere with necks making contact with the Brillouin-zone boundary around L. The neck areas given in the table are somewhat larger than implied by the experimental results of Tsui.[29] It is probable that the L_2' level has been placed slightly too far below the Fermi energy.

The minority-spin portion of the Fermi surface is considerably more complicated. In the first place, we find the hole pockets at X which have been observed in measurements of the de Haas–van Alphen effect. Our results for the size of this pocket, which is associated with the X_5 level, are in rather good agreement with the measurements.

We also find a second pocket of minority-spin holes ($3d$ band) near X associated with the X_2 level. Such holes have not been observed experimentally, although they have been predicted by other first-principles calculations as well.[11] If there are, in fact, no such holes, the discrepancy could be ex-

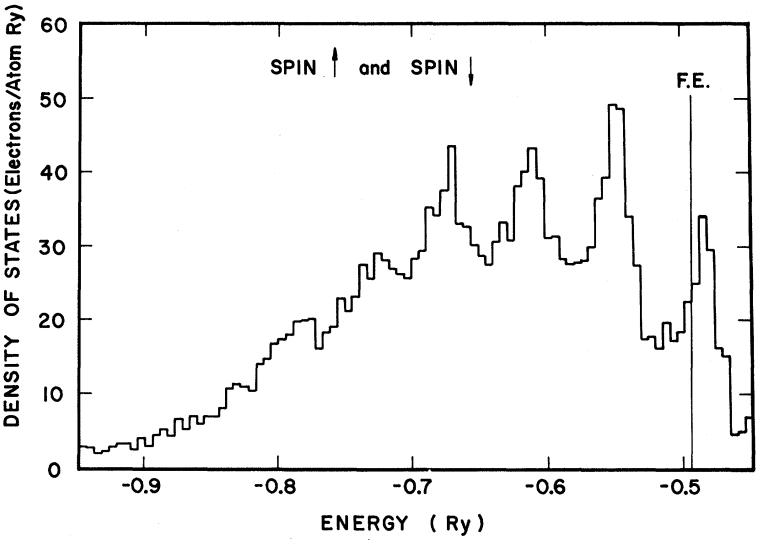

FIG. 7. Total density of states.

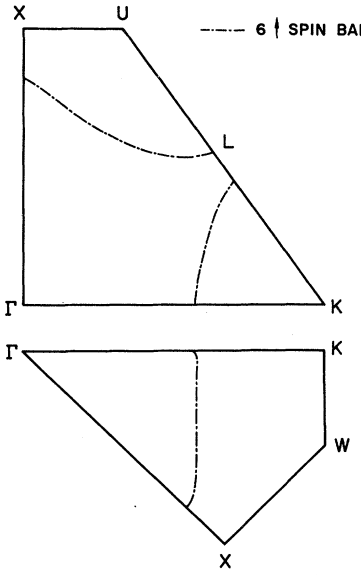

FIG. 8. Fermi-surface contours for states of majority spin in certain planes.

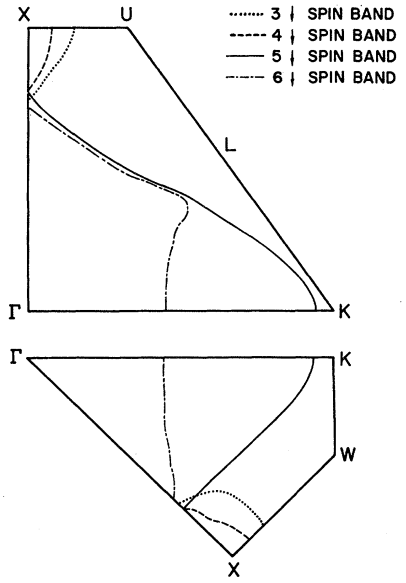

FIG. 9. Fermi-surface contours for states of minority spin in certain planes. Bands are labeled according to their order at X.

plained by a slightly too-low placement of the Fermi Fermi level in our calculation; the actual position of the Fermi level would then come between X_5 and X_2.

There are large portions of the minority-spin Fermi surface which have not yet been observed: that associated with the band-5 holes presumably responsible for the ferromagnetism and the band-6 electrons. Measurement of the properties of these portions of the Fermi surface would be of considerable importance in testing band calculations.

We have also computed the spin-wave reciprocal effective mass in the following way. The energy of a long-wavelength spin wave of wave vector q can be expressed as

$$E = Dq^2 . \tag{4.1}$$

The coefficient D can be determined approximately from[15,30]

$$D = \frac{\Omega}{6(2\pi)^3} \sum_l \int d^3k \left(\nabla^2 \epsilon_l(\vec{k}) - \frac{2 \mid \nabla \epsilon_l(\vec{k}) \mid^2}{U_l(\vec{k})} \right) d^3k \tag{4.2}$$

in which $\epsilon_l(\vec{k})$ is the energy of a state of wave vector $\vec{k}$ in band l. In application to nickel to d-band holes, the integral is then to include occupied hole states. The function $U_l(\vec{k})$ is the spin splitting,

$$U_l(\vec{k}) = \epsilon_{l\uparrow}(\vec{k}) - \epsilon_{l\downarrow}(\vec{k}) . \tag{4.3}$$

The integral (4.2) has been calculated using a grid of 1505 points in $\frac{1}{48}$th of the zone. The result is, in atomic units, $D = 0.165$, which can be compared with the experimental results of Stringfellow,[31] extrapolated to $T = 0$; $D = 0.12$. The discrepancy may perhaps be primarily due to the fact, noted previously, that the calculated spin splitting is too large.

The present calculation has yielded reasonable results for the band structure and related properties of ferromagnetic nickel. We are presently attempting to improve the calculation by making it self consistent,[20] and through the inclusion of spin-orbit coupling.

APPENDIX A

In this Appendix we present expressions for the integrals used in the computation of the matrix elements of the kinetic energy and the potential energy. The latter require elements of $\cos(\vec{K}_\nu \cdot \vec{r}_C)$. The wave functions are linear combinations of GTO's. The matrix elements of the unit operator, which are the overlap integrals, are obtained by setting $\vec{K}_\nu = 0$ in the potential integrals. Only independent

TABLE III. Properties of the Fermi surface.

	Symmetry axis	Extremal area (a.u.)	m^*/m_0
$L_2'(\uparrow)$ neck	(111)	0.0093	0.09
$X_5(\downarrow)$ hole pocket	(100)	0.020	0.14
	ΓXW plane	0.055	
$X_2(\downarrow)$ hole pocket	(100)	0.061	1.23
	ΓXW plane	0.096	

expressions are given; others can be obtained by appropriate permutations. The notation is such that

$$\langle i \mid \hat{O} \mid j \rangle = \langle G^{(i)}(\alpha_1, \vec{r} - \vec{A}) \mid \hat{O} \mid G^{(j)}(\alpha_2, \vec{r} - \vec{B}) \rangle ,$$

where $G^{(i)}(\alpha, \vec{r} - \vec{A})$ denotes a Gaussian orbital. The index i defines a specified row of one of the irreducible representations of the cubic point group. We write

$$G^{(i)}(\vec{r}) = R_l(r) K_i(\theta, \phi) ,$$

in which $K_i(\theta, \phi)$ is a cubic harmonic and $R_l(r)$ is a radial function ($l = 0, 1, 2$), where

$$R_l(r) = r^l e^{-\alpha r^2} .$$

Only $\langle s \mid \hat{O} \mid d \rangle$, $\langle p \mid \hat{O} \mid d \rangle$, and $\langle d \mid \hat{O} \mid d \rangle$ integrals are given, since the expressions for $\langle s \mid \hat{O} \mid s \rangle$, $\langle p \mid \hat{O} \mid s \rangle$, and $\langle p \mid \hat{O} \mid p \rangle$ have been given by Chaney *et al.*[21] We can derive all subsequent integrals from $\langle s \mid \hat{O} \mid s \rangle$, where $\hat{O}$ is one of the operators $-\nabla^2$ or $\cos(\vec{K}_\nu \cdot \vec{r}_C)$. As examples of this, we have

$$\langle P_x \mid \hat{O} \mid s \rangle = \frac{1}{2\alpha_1} \frac{d}{dA_x} \langle s \mid \hat{O} \mid s \rangle ,$$

$$\langle P_x \mid \hat{O} \mid P_x \rangle = \frac{1}{2\alpha_2} \frac{d}{dB_x} \langle P_x \mid \hat{O} \mid s \rangle ,$$

$$\langle d_{(x^2-y^2)} \mid \hat{O} \mid s \rangle = \frac{1}{2\alpha_1} \frac{d}{dA_x} \langle P_x \mid \hat{O} \mid s \rangle - \frac{1}{2\alpha_1} \frac{d}{dA_y} \langle P_y \mid \hat{O} \mid s \rangle .$$

The following abbreviations are used below:

$$u = \frac{\alpha_1}{\alpha_1 + \alpha_2} , \quad \lambda = \frac{\alpha_1 \alpha_2}{\alpha_1 + \alpha_2} , \quad \Delta = \left(\frac{\pi}{\alpha_1 + \alpha_2} \right)^{3/2} ,$$

$$\delta = \exp\left(\frac{-K_\nu^2}{4(\alpha_1 + \alpha_2)} \right) , \quad W = \frac{1}{\alpha_1 + \alpha_2} , \quad \xi = e^{-\lambda R^2} ,$$

$$X = B_x - A_x , \qquad Y = B_y - A_y ,$$

$$Z = B_z - A_z , \qquad R^2 = X^2 + Y^2 + Z^2 .$$

The expressions given here must be multiplied by the appropriate constants resulting from normalization of the radial functions and the spherical harmonics:

$$\langle s \mid -\nabla^2 \mid d_{xy} \rangle = 2\Delta\xi W^2 \alpha_1^2 \lambda XY (7 - 2\lambda R^2) ,$$

$$\langle s \mid \cos(\vec{K}_\nu \cdot \vec{r}_C) \mid d_{xy} \rangle = \Delta\delta\xi W^2 [(\alpha_1^2 XY - \tfrac{1}{4} K_{\nu x} K_{\nu y}) \cos(\vec{K}_\nu \cdot \vec{r}_{CD}) + \tfrac{1}{2} \alpha_1 (YK_{\nu x} + XK_{\nu y}) \sin(\vec{K}_\nu \cdot \vec{r}_{CD})] ,$$

$$\langle s \mid -\nabla^2 \mid d_{(x^2-y^2)} \rangle = 2\Delta\xi W^2 \alpha_1^2 \lambda (X^2 - Y^2)(7 - 2\lambda R^2) ,$$

$$\langle s \mid \cos(\vec{K}_\nu \cdot \vec{r}_C) \mid d_{(x^2-y^2)} \rangle = \Delta\delta\xi W^2 \{ [\alpha_1^2 (X^2 - Y^2) - \tfrac{1}{4} (K_{\nu x}^2 K_{\nu y}^2)] \cos(\vec{K}_\nu \cdot \vec{r}_{CD}) + \alpha_1 (XK_{\nu x} - YK_{\nu y}) \sin(\vec{K}_\nu \cdot \vec{r}_{CD}) \} ,$$

$$\langle s \mid -\nabla^2 \mid d_{(3z^2-r^2)} \rangle = 2\Delta\xi W^2 \alpha_1^2 \lambda (2Z^2 - X^2 - Y^2)(7 - 2\lambda R^2) ,$$

$$\langle s \mid \cos(\vec{K}_\nu \cdot \vec{r}_C) \mid d_{(3z^2-r^2)} \rangle = \Delta\delta\xi W^2 \{ [\alpha_1^2 (2Z^2 - X^2 - Y^2) - \tfrac{1}{4} (2K_{\nu z}^2 - K_{\nu x}^2 - K_{\nu y}^2)] \cos(\vec{K}_\nu \cdot \vec{r}_{CD}) + \alpha_1 (2ZK_{\nu z} - XK_{\nu x} - YK_{\nu y}) \sin(\vec{K}_\nu \cdot \vec{r}_{CD}) \} ,$$

$$\langle P_x \mid -\nabla^2 \mid d_{xy} \rangle = 2\Delta\xi W^2 \alpha_1 \lambda (\tfrac{7}{2} - 9\lambda X^2 - \lambda R^2 + 2\lambda^2 X^2 R^2) ,$$

$$\langle P_x \mid \cos(\vec{K}_\nu \cdot \vec{r}_C) \mid d_{xy} \rangle = \Delta\delta\xi W^2 \{ [\tfrac{1}{4} K_{\nu x} K_{\nu y} X(2u - 1) + \tfrac{1}{2} \alpha_1 Y - \tfrac{1}{4} \alpha_1 K_{\nu x}^2 WY - \alpha_1 \lambda X^2 Y] \cos(\vec{K}_\nu \cdot \vec{r}_{CD}) + [\tfrac{1}{2} \alpha_1 K_{\nu x} XY(1 - 2u) + \tfrac{1}{4} K_{\nu y} - \tfrac{1}{2} \lambda K_{\nu y} X^2 - \tfrac{1}{8} K_{\nu y} K_{\nu x}^2 W] \sin(\vec{K}_\nu \cdot \vec{r}_{CD}) \} ,$$

$$\langle P_z \mid -\nabla^2 \mid d_{xy} \rangle = 2\Delta\xi W^3 \lambda \alpha_1^2 \alpha_2 XYZ (2\lambda R^2 - 9),$$

$$\langle P_z \mid \cos\vec{K}_\nu \cdot \vec{r}_C \mid d_{xy} \rangle = \Delta\delta\xi W^3 \{ [\alpha_2 Z (\tfrac{1}{4} K_{\nu x} K_{\nu y} - \alpha_1^2 XY) - \tfrac{1}{4} \alpha_1 K_{\nu z} (XK_{\nu y} + YK_{\nu x})] \cos(\vec{K}_\nu \cdot \vec{r}_{CD}) + \tfrac{1}{2} [K_{\nu z} (\alpha_1^2 XY - \tfrac{1}{4} K_{\nu x} K_{\nu y}) - \alpha_1 \alpha_2 Z (YK_{\nu x} + XK_{\nu y})] \sin(\vec{K}_\nu \cdot \vec{r}_{CD}) \} ,$$

$$\langle P_z \mid -\nabla^2 \mid d_{(x^2-y^2)} \rangle = 2\Delta\xi W^3 \lambda \alpha_1^2 \alpha_2 Z (X^2 - Y^2)(2\lambda R^2 - 9) ,$$

$$\langle P_z \mid \cos(\vec{K}_\nu \cdot \vec{r}_C) \mid d_{(x^2-y^2)} \rangle = \Delta\delta\xi W^3 (\{ \alpha_2 Z [\tfrac{1}{4} (K_{\nu x}^2 - K_{\nu y}^2) - \alpha_1^2 (X^2 - Y^2)] - \tfrac{1}{2} \alpha_1 K_{\nu z} (XK_{\nu x} - YK_{\nu y}) \} \cos(\vec{K}_\nu \cdot \vec{r}_{CD}) + \{ \tfrac{1}{2} K_{\nu z} [\alpha_1^2 (X^2 - Y^2) - \tfrac{1}{4} (K_{\nu x}^2 - K_{\nu y}^2)] - \alpha_1 \alpha_2 Z (XK_{\nu x} - YK_{\nu y}) \} \sin(\vec{K}_\nu \cdot \vec{r}_{CD})),$$

$$\langle P_x \mid -\nabla^2 \mid d_{(x^2-y^2)} \rangle = 2\Delta\xi W^2 \lambda \alpha_1 X [7 - 2\lambda R^2 + (X^2 - Y^2)(2\lambda^2 R^2 - 9\lambda)] ,$$

$$\langle P_x \mid \cos(\vec{K}_\nu \cdot \vec{r}_C) \mid d_{(x^2-y^2)} \rangle = \Delta\delta\xi W^3 (\{ \alpha_2 X [\tfrac{1}{4} (K_{\nu x}^2 - K_{\nu y}^2) - \alpha_1^2 (X^2 - Y^2)] - \tfrac{1}{2} \alpha_1 K_{\nu x} (XK_{\nu x} - YK_{\nu y}) + \alpha_1 X / W \} \times \cos(\vec{K}_\nu \cdot \vec{r}_{CD}) + \{ \tfrac{1}{2} K_{\nu x} [\alpha_1^2 (X^2 - Y^2) - \tfrac{1}{4} (K_{\nu x}^2 - K_{\nu y}^2) + 1/W] - \alpha_1 \alpha_2 X (XK_{\nu x} - YK_{\nu y}) \} \sin(\vec{K}_\nu \cdot \vec{r}_{CD})) ,$$

$$\langle P_x \mid -\nabla^2 \mid d_{(3z^2-r^2)}\rangle = 2\Delta\xi W^2\lambda\alpha_1 X[2\lambda R^2 - 7 + (2\lambda^2R^2 - 9\lambda)(2Z^2 - X^2 - Y^2)],$$

$$\langle P_x \mid \cos\vec{K}_\nu\cdot\vec{r}_C \mid d_{(3z^2-r^2)}\rangle = \Delta\delta\xi W^3\{[\tfrac{1}{4}\alpha_2 X(2K_{\nu z}^2 - K_{\nu x}^2 - K_{\nu y}^2) - \alpha_1^2\alpha_2 X(2Z^2 - X^2 - Y^2) - \tfrac{1}{2}\alpha_1 K_{\nu x}(2ZK_{\nu z} - XK_{\nu x} - YK_{\nu y}) - \alpha_1 X/W]\cos(\vec{K}_\nu\cdot\vec{r}_{CD}) + [\tfrac{1}{2}K_{\nu x}\alpha_1^2(2Z^2 - X^2 - Y^2) - \tfrac{1}{2}K_{\nu x}/W - \tfrac{1}{8}K_{\nu x}(2K_{\nu z}^2 - K_{\nu x}^2 - K_{\nu y}^2) - \alpha_1\alpha_2 X(2ZK_{\nu z} - XK_{\nu x} - YK_{\nu y})]\sin(\vec{K}_\nu\cdot\vec{r}_{CD})\},$$

$$\langle P_z \mid -\nabla^2 \mid d_{(3z^2-r^2)}\rangle = 2\Delta\xi W^2\lambda\alpha_1 Z[(2\lambda^2R^2 - 9\lambda)(2Z^2 - X^2 - Y^2) + 2(7 - 2\lambda R^2)],$$

$$\langle P_z \mid \cos\vec{K}_\nu\cdot\vec{r}_C \mid d_{(3z^2-r^2)}\rangle = \Delta\delta\xi W^3\{[\tfrac{1}{4}\alpha_2 Z(2K_{\nu z}^2 - K_{\nu x}^2 - K_{\nu y}^2) - \alpha_1^2\alpha_2 Z(2Z^2 - X^2 - Y^2) - \tfrac{1}{2}\alpha_1 K_{\nu z}(2ZK_{\nu z} - XK_{\nu x} - YK_{\nu y}) + 2\alpha_1 Z/W]\cos(\vec{K}_\nu\cdot\vec{r}_{CD}) + [K_{\nu z}/W + \tfrac{1}{2}\alpha_1^2 K_{\nu z}(2Z^2 - X^2 - Y^2) - \tfrac{1}{8}K_{\nu z}(2K_{\nu z}^2 - K_{\nu x}^2 - K_{\nu y}^2) - \alpha_1\alpha_2 Z(2ZK_{\nu z} - XK_{\nu x} - YK_{\nu y})]\sin(\vec{K}_\nu\cdot\vec{r}_{CD})\},$$

$$\langle d_{xy} \mid -\nabla^2 \mid d_{xy}\rangle = 2\Delta\xi W^2\lambda[(\tfrac{7}{2} - 9\lambda Y^2)(1 - 2\lambda X^2) + (2\lambda^2Y^2 - \lambda)(2X^2 + R^2 - 2\lambda X^2R^2)],$$

$$\langle d_{xy} \mid \cos(\vec{K}_\nu\cdot\vec{r}_C) \mid d_{xy}\rangle = \Delta\delta\xi W^3\{[\alpha_1\alpha_2\lambda X^2Y^2 + \tfrac{1}{4}\lambda(Y^2K_{\nu x}^2 + X^2K_{\nu y}^2) - \tfrac{1}{4}W(\alpha_1 - \alpha_2)^2 XYK_{\nu x}K_{\nu y} - \tfrac{1}{8}(K_{\nu x}^2 + K_{\nu y}^2) - \tfrac{1}{2}\alpha_1\alpha_2(X^2 + Y^2) + \tfrac{1}{16}K_{\nu x}^2K_{\nu y}^2W + 1/4W]\cos(\vec{K}_\nu\cdot\vec{r}_{CD}) + \tfrac{1}{2}(\alpha_2 - \alpha_1)[(\lambda XY + \tfrac{1}{4}WK_{\nu x}K_{\nu y})(YK_{\nu x} + XK_{\nu y}) - \tfrac{1}{2}(XK_{\nu x} + YK_{\nu y})]\sin\vec{K}_\nu\cdot\vec{r}_{CD}\},$$

$$\langle d_{xz} \mid -\nabla^2 \mid d_{xy}\rangle = 2\Delta\xi W^2\lambda^2 YZ(-\tfrac{9}{2} + 11X\lambda + \lambda R^2 - 2\lambda^2X^2R^2),$$

$$\langle d_{xz} \mid \cos(\vec{K}_\nu\cdot\vec{r}_C) \mid d_{xy}\rangle = \Delta\delta\xi W^3([\alpha_1\alpha_2\lambda X^2YZ + \tfrac{1}{4}\lambda(YZK_{\nu x}^2 + X^2K_{\nu y}K_{\nu z}) + \tfrac{1}{4}(1 - 2u)XK_{\nu x}(\alpha_2 ZK_{\nu y} - \alpha_1 YK_{\nu z}) - \tfrac{1}{8}K_{\nu y}K_{\nu z} - \tfrac{1}{2}\alpha_1\alpha_2 YZ + \tfrac{1}{16}WK_{\nu x}^2K_{\nu y}K_{\nu z}]\cos(\vec{K}_\nu\cdot\vec{r}_{CD}) + \{\tfrac{1}{2}\lambda[XYZK_{\nu x}(\alpha_2 - \alpha_1) + \alpha_2X^2ZK_{\nu y} - \alpha_1X^2YK_{\nu z}] + \tfrac{1}{8}WK_{\nu x}^2(\alpha_2 ZK_{\nu y} - \alpha_1 YK_{\nu z}) + \tfrac{1}{8}W(\alpha_2 - \alpha_1)XK_{\nu x}K_{\nu y}K_{\nu z} + \tfrac{1}{4}(\alpha_1 YK_{\nu z} - \alpha_2 ZK_{\nu y})\}\sin(\vec{K}_\nu\cdot\vec{r}_{CD})),$$

$$\langle d_{xy} \mid -\nabla^2 \mid d_{(x^2-y^2)}\rangle = 2\Delta\xi W^2\lambda^3 XY(X^2 - Y^2)(11 - 2\lambda R^2),$$

$$\langle d_{xy} \mid \cos(\vec{K}_\nu\cdot\vec{r}_C) \mid d_{(x^2-y^2)}\rangle = \Delta\delta\xi W^3(\{(X^2 - Y^2)[\alpha_1\alpha_2 XY + \tfrac{1}{2}\alpha_1 W(\alpha_2 - \tfrac{1}{2}\alpha_1)K_{\nu x}K_{\nu y}] + (K_{\nu x}^2 - K_{\nu y}^2) \times [\tfrac{1}{2}\alpha_2 W(\alpha_1 - \tfrac{1}{2}\alpha_2)XY + \tfrac{1}{16}WK_{\nu x}K_{\nu y}]\}\cos(\vec{K}_\nu\cdot\vec{r}_{CD}) + \{(XK_{\nu y} + YK_{\nu x})[\tfrac{1}{8}\alpha_2 W(K_{\nu x}^2 - K_{\nu y}^2) - \tfrac{1}{2}\alpha_1\lambda(X^2 - Y^2)] + \tfrac{1}{2}(\alpha_1 + \alpha_2)(XK_{\nu y} - YK_{\nu x}) + (XK_{\nu x} - YK_{\nu y})(\alpha_2\lambda XY - \tfrac{1}{4}\alpha_1 WK_{\nu x}K_{\nu y})\}\sin(\vec{K}_\nu\cdot\vec{r}_{CD})),$$

$$\langle d_{xz} \mid -\nabla^2 \mid d_{(3z^2-r^2)}\rangle = 2\Delta\xi W^2\lambda^2 XZ[2\lambda R^2 - 9 + \lambda(11 - 2\lambda R^2)(2Z^2 - X^2 - Y^2)],$$

$$\langle d_{xz} \mid \cos(\vec{K}_\nu\cdot\vec{r}_C) \mid d_{(3z^2-r^2)}\rangle = \Delta\delta\xi W^3([(2Z^2 - Y^2 - X^2)(\alpha_1\alpha_2\lambda XZ - \tfrac{1}{4}\alpha_1^2K_{\nu x}K_{\nu z}W) + \tfrac{1}{4}W(\tfrac{1}{4}K_{\nu x}K_{\nu z} - \alpha_2^2XZ) \times(2K_{\nu z}^2 - K_{\nu x}^2 - K_{\nu y}^2) - \alpha_1\alpha_2XZ - \tfrac{1}{4}K_{\nu x}K_{\nu z} + \tfrac{1}{2}\lambda(XK_{\nu z} + ZK_{\nu x})(2ZK_{\nu z} - XK_{\nu x} - YK_{\nu y})]\cos(\vec{K}_\nu\cdot\vec{r}_{CD}) + \{(XK_{\nu z} + ZK_{\nu x})[\tfrac{1}{8}\alpha_2 W(2K_{\nu z}^2 - K_{\nu x}^2 - K_{\nu y}^2) - \tfrac{1}{2}\alpha_1\lambda(2Z^2 - X^2 - Y^2)] - (\alpha_2 + \tfrac{1}{2}\alpha_1)XK_{\nu z} + (\alpha_1 + \tfrac{1}{2}\alpha_2)ZK_{\nu x} + (2ZK_{\nu z} - XK_{\nu x} - YK_{\nu y})(\alpha_2\lambda XZ - \tfrac{1}{4}W\alpha_1K_{\nu x}K_{\nu z})\}\sin(\vec{K}_\nu\cdot\vec{r}_{CD})),$$

$$\langle d_{(x^2-y^2)} \mid -\nabla^2 \mid d_{(x^2-y^2)}\rangle = 2\Delta\xi W^2\lambda\{4 + 8\lambda^2(X^2 - Y^2)^2 - 12\lambda(X^2 + Y^2) + (3 - 2\lambda R^2)[\lambda^2(X^2 - Y^2)^2 - 2\lambda(X^2 + Y^2) + 1]\},$$

$$\langle d_{(x^2-y^2)} \mid \cos(\vec{K}_\nu\cdot\vec{r}_C) \mid d_{(x^2-y^2)}\rangle = \Delta\delta\xi W^4([\alpha_1^2\alpha_2^2(X^2 - Y^2)^2 - \tfrac{1}{4}(\alpha_1^2 + \alpha_2^2)(X^2 - Y^2)(K_{\nu x}^2 - K_{\nu y}^2) + \alpha_1\alpha_2 \times(XK_{\nu x} - YK_{\nu y})^2 - 2\alpha_1\alpha_2(X^2 + Y^2)/W + \tfrac{1}{16}(K_{\nu x}^2 - K_{\nu y}^2)^2 - \tfrac{1}{2}(K_{\nu x}^2 + K_{\nu y}^2)/W + 1/W^2]\cos(\vec{K}_\nu\cdot\vec{r}_{CD}) + \{(\alpha_2 - \alpha_1) \times(XK_{\nu x} - YK_{\nu y})[\alpha_1\alpha_2(X^2 - Y^2) + \tfrac{1}{4}(K_{\nu x}^2 - K_{\nu y}^2)] - (\alpha_2 - \alpha_1)(XK_{\nu x} + YK_{\nu y})/W\}\sin(\vec{K}_\nu\cdot\vec{r}_{CD})),$$

$$\langle d_{(x^2-y^2)} \mid -\nabla^2 \mid d_{(3z^2-r^2)}\rangle = 2\Delta\xi W^2\lambda^2(X^2 - Y^2)[18 - 4\lambda R^2 + \lambda(11 - 2\lambda R^2)(2Z^2 - X^2 - Y^2)],$$

$$\langle d_{(x^2-y^2)} \mid \cos(\vec{K}_\nu\cdot\vec{r}_C) \mid d_{(3z^2-r^2)}\rangle = \Delta\delta\xi W^3(\{\tfrac{1}{4}W[\tfrac{1}{4}(K_{\nu x}^2 - K_{\nu y}^2) - \alpha_2^2(X^2 - Y^2)](2K_{\nu z}^2 - K_{\nu x}^2 - K_{\nu y}^2) + W(2Z^2 - X^2 - Y^2) \times[\alpha_1^2\alpha_2^2(X^2 - Y^2) - \tfrac{1}{4}\alpha_1^2(K_{\nu x}^2 - K_{\nu y}^2)] + 2\alpha_1\alpha_2(X^2 - Y^2) + \lambda(2ZK_{\nu z} - XK_{\nu x} - YK_{\nu y})(XK_{\nu x} - YK_{\nu y}) + \tfrac{1}{2}(K_{\nu x}^2 - K_{\nu y}^2)\}\cos(\vec{K}_\nu\cdot\vec{r}_{CD}) + \{(XK_{\nu x} - YK_{\nu y})[\tfrac{1}{4}\alpha_2 W(2K_{\nu z}^2 - K_{\nu x}^2 - K_{\nu y}^2) - \alpha_1\lambda(2Z^2 - X^2 - Y^2) + (\alpha_2 - \alpha_1)] + (2ZK_{\nu z} - XK_{\nu x} - YK_{\nu y})[\alpha_2\lambda(X^2 - Y^2) - \tfrac{1}{4}\alpha_1 W(K_{\nu x}^2 - K_{\nu y}^2)]\}\sin(\vec{K}_\nu\cdot\vec{r}_{CD})),$$

TABLE IV. d–d tight-binding integrals.

Integral	Neighbor	Kinetic plus potential energy (Ry)	Exchange (Ry)	Overlap
$d_{(3z^2-r^2)}$, $d_{(3z^2-r^2)}$	(0, 0, 0)	3.098	−3.784	1.000
$d_{(3z^2-r^2)}$, $d_{(3z^2-r^2)}$	(1, 1, 0)	−0.006 663	−0.005 573	0.004 558
$d_{(3z^2-r^2)}$, $d_{(3z^2-r^2)}$	(0, 0, 2)	−0.001 685	−0.000 158 9	0.000 308 4
$d_{(x^2-y^2)}$, $d_{(x^2-y^2)}$	(0, 0, 0)	3.098	−3.784	1.000
$d_{(x^2-y^2)}$, $d_{(x^2-y^2)}$	(1, 1, 0)	0.012 34	0.005 775	−0.005 819
$d_{(x^2-y^2)}$, $d_{(x^2-y^2)}$	(0, 0, 2)	−0.0000 197 4	−0.000 003 06	0.000 002 427
d_{xy}, d_{xy}	(0, 0, 0)	3.906	−3.788	1.000
d_{xy}, d_{xy}	(1, 1, 0)	−0.016 81	−0.016 08	0.012 54
d_{xy}, d_{xy}	(0, 0, 2)	−0.000 018 57	−0.000 002 352	0.000 002 427
d_{xz}, d_{xz}	(0, 0, 0)	3.096	−3.788	1.000
d_{xz}, d_{xz}	(1, 1, 0)	0.005 401	0.002 811	−0002 626
d_{xz}, d_{xz}	(0, 0, 2)	0.000 333 2	0.000 043 7	−0.000 049 84
d_{yz}, d_{xz}	(1, 1, 0)	0.007 073	0.003 399	−0.003 194
d_{xy}, $d_{(3z^2-r^2)}$	(1, 1, 0)	0.008 725	0.008 919	−0.006 911

$$\langle d_{(3z^2-r^2)} | -\nabla^2 | d_{(3z^2-r^2)} \rangle = 2\Delta\xi W^2\lambda[21 - 6\lambda R^2 + 2\lambda(2R^2-9)(X^2+Y^2+4Z^2) + \lambda^2(11 - 2\lambda R^2)(2Z^2 - X^2 - Y^2)^2] ,$$

$$\langle d_{(3z^2-r^2)} | \cos(\vec{K}_\nu \cdot \vec{r}_C) | d_{(3z^2-r^2)} \rangle = \Delta\delta\xi W^3([\alpha_1\alpha_2\lambda(2Z^2 - X^2 - Y^2)^2 - 2\alpha_1\alpha_2(4Z^2 + X^2 + Y^2) + 3/W$$
$$- \tfrac{1}{4}W(\alpha_1^2 + \alpha_2^2)(2Z^2 - X^2 - Y^2)(2K_{\nu z}^2 - K_{\nu x}^2 - K_{\nu y}^2) + \lambda(2ZK_{\nu z} - XK_{\nu x} - YK_{\nu y})^2 + \tfrac{1}{16}W(2K_{\nu z}^2 - K_{\nu x}^2 - K_{\nu y}^2)^2$$
$$- \tfrac{1}{2}(4K_{\nu z}^2 + K_{\nu x}^2 + K_{\nu y}^2)] \cos(\vec{K}_\nu \cdot \vec{r}_{CD}) + (\alpha_2 - \alpha_1)\{(2ZK_{\nu z} - XK_{\nu x} - YK_{\nu y})[\lambda(2Z^2 - X^2 - Y^2)$$
$$+ \tfrac{1}{4}W(2K_{\nu z}^2 - K_{\nu x}^2 - K_{\nu y}^2)] - (4ZK_{\nu z} + XK_{\nu x} + YK_{\nu y})\} \sin(\vec{K}_\nu \cdot \vec{r}_{CD})) .$$

APPENDIX B

In this Appendix, we present numerical values for integrals of importance for conventional tight-binding calculations for d bands. These quantities are the matrix elements $E_{jn}(\vec{R}_\mu)$ [see Eq. (2.8)] in which j and n are d states, for central cell, first, and second neighbors [$R_\mu = 0$, $\frac{1}{2}a(1, 1, 0)$, $\frac{1}{2}a(0, 0, 2)$]. Values a given in Table IV for the sum of kinetic energy and ordinary (Coulomb) potential energy, the exchange energy (full Slater for the paramagnetic state), and overlap integrals. These integrals were determined using the atomic wave functions of Wachters.[22] In the calculations described in the main text of this paper, we used Bloch functions formed from individual Gaussian orbitals rather than complete atomic wave functions; however, integrals based on atomic wave functions are interesting for purposes of comparison with values obtained by various interpolation schemes. In this connection, it should be noted that values for these quantities previously reported by this group[32] based on Slater orbitals are in error.

Many authors have considered the so-called two-center approximation,[33] in which three-center integrals occurring in the usual form of the tight-binding method are neglected. There are several different combinations of the integrals E_{jn} which can be used to determine values of the two-center integrals $(dd\sigma)$, $(dd\pi)$, $(dd\delta)$. The results would agree if the two-center approximations were accurate. In the present case, the spread is not large for first neighbors except in the case of the integral of smallest magnitude, $(dd\delta)$. Mean values for the nearest-neighbor two-center parameters obtained from Table IV are presented in Table V, where they are compared with those obtained by other authors. There is some measure of agreement with the values obtained by fits to APW cal-

TABLE V. Comparison of two-center integrals. All values are in rydbergs.

Type	Present results ($\alpha = 1$)	Fletcher and Wohlfarth[a]	Hodges and Ehrenreich[b]	Zornberg[c]
$dd\sigma$	−0.0428	−0.0248	−0.0384	−0.038
$dd\pi$	0.0186	0.0134	0.0228	0.017
$dd\delta$	−0.0022	−0.0019	−0.0056	−0.0017

[a]Reference 1.
[b]From three-center fit to APW calculation (Ref. 13).
[c]From two-center fit to APW calculation (Ref. 14).

culations. The substantial discrepancies with the values of Fletcher and Wohlfarth would be substantially reduced if the contribution from the exchange potential to our values was deleted. Fletcher and Wohlfarth did not include exchange in their calculations.

†Work supported in part by the U. S. Air Force Office of Scientific Research under Grant No. AF 68-1565.

[1]G. C. Fletcher and E. P. Wohlfarth, Phil. Mag. 42, 106 (1951).
[2]G. C. Fletcher, Proc. Phys. Soc. (London) A65, 192 (1952).
[3]J. G. Hanus, MIT Solid State and Molecular Theory Group Quarterly Progress Report No. 44, p. 29, 1962 (unpublished).
[4]J. Yamashita, M. Fukuchi, and S. Wakeh, J. Phys. Soc. Japan 18, 999 (1963).
[5]S. Wakoh and J. Yamashita, J. Phys. Soc. Japan 19, 1342 (1964).
[6]L. F. Mattheiss, Phys. Rev. 134, A970 (1964).
[7]S. Wakoh, J. Phys. Soc. Japan 20, 1894 (1965).
[8]E. C. Snow, J. T. Waber, and A. C. Switendick, J. Appl. Phys. 37, 1342 (1966).
[9]L. Hodges, H. Ehrenreich, and N. D. Lang, Phys. Rev. 152, 505 (1966).
[10]F. M. Mueller, Phys. Rev. 153, 659 (1967).
[11]J. W. D. Connolly, Phys. Rev. 159, 415 (1967).
[12]J. Ruvalds and L. M. Falicov, Phys. Rev. 172, 508 (1968).
[13]H. Ehrenreich and L. Hodges, Methods Comput. Phys. 8, 149 (1968).
[14]E. Zornberg, Phys. Rev. B 1, 2411 (1970).
[15]J. Callaway and H. M. Zhang, Phys. Rev. B 1, 305 (1970).
[16]J. Callaway, H. M. Zhang, T. E. Norwood, and J. Langlinais, Intern. J. Quantum Chem. 4, 425 (1971).
[17]J. Callaway and D. M. Edwards, Phys. Rev. 118, 923 (1960).
[18]E. Lafon and C. C. Lin, Phys. Rev. 152, 597 (1966).
[19]J. C. Slater, T. M. Wilson, and J. H. Wood, Phys. Rev. 179, 28 (1969).
[20]J. Callaway and J. L. Fry, in *Computational Methods in Band Theory*, edited by P. M. Marcus, D. F. Janak, and A. R. Williams (Plenum, New York, 1971), p. 512.
[21]R. C. Chaney, T. K. Tung, C. C. Lin, and E. Lafon, J. Chem. Phys. 52, 361 (1970).
[22]A. J. H. Wachters, J. Chem. Phys. 52, 1033 (1970).
[23]E. Clementi, *Tables of Atomic Functions* (IBM Corp., San Jose, Calif., 1965).
[24]J. C. Slater, Phys. Rev. 81, 385 (1951).
[25]W. Kohn and L. J. Shaw, Phys. Rev. 140, A1133 (1965).
[26]J. Callaway, Phys. Rev. 99, 500 (1955).
[27]C. Herring, *Exchange Interactions Among Itinerant Electrons* (Academic, New York, 1966).
[28]H. Dannan, A. Heer, and A. J. P. Meyer, J. Appl. Phys. 39, 669 (1968).
[29]D. C. Tsui, Phys. Rev. 164, 669 (1967).
[30]D. M. Edwards, Proc. Roy. Soc. (London) A300, 373 (1967).
[31]M. W. Stringfellow, J. Phys. C 1, 950 (1968).
[32]J. M. Tyler, T. E. Norwood, and J. L. Fry, Phys. Rev. B 1, 297 (1970).
[33]J. C. Slater and G. F. Koster, Phys. Rev. 94, 1498 (1954).

PHYSICAL REVIEW B VOLUME 5, NUMBER 1 1 JANUARY 1972

Hyperfine Magnetic Field of Argon Implanted in Nickel

H. G. Devare* and H. de Waard
Natuurkundig Laboratorium der Rijksuniversiteit, Groningen, The Netherlands
(Received 20 July 1971)

The hyperfine field of argon in nickel is measured to be 280 ±23 kG using the technique of time-differential perturbed angular correlations. The argon nuclei were recoil implanted in nickel by the ^{39}K(d, α) ^{37}Ar reaction. The second excited state of ^{37}Ar at 1610 keV was used in this measurement. The unperturbed α_2–1610-keV γ-ray angular correlation was studied with a copper backing for the target, and values $A_2 = 0.265 \pm 0.057$ and $A_4 = -0.222 \pm 0.098$ were obtained for the correlation coefficients. The amplitude of modulation of the time spectrum is found to be very small. This may be interpreted by assuming that the hyperfine field acts only on a small fraction of the implanted nuclei.

I. INTRODUCTION

At present, hardly any data exist about the hyperfine magnetic fields acting on nuclei with $Z < 20$ imbedded in ferromagnetic lattices. A knowledge of these fields is of interest not only because of their utility in measuring magnetic moments of short-lived nuclear excited states, but also for understanding the mechanism which produces these fields. We report here on a measurement of the magnetic field on Ar nuclei in nickel. This measurement is of particular significance because Ar is an inert gas with a closed electron shell. This simple electron configuration should facilitate the calculation of the magnetic hyperfine field, which is believed to be largely due to overlap polarization.